ESTIMATION OF PM_{10}-BOUND MANGANESE CONCENTRATION NEAR A FERROMANGANESE ALLOY PLANT BY ATMOSPHERIC DISPERSION MODELLING

Daniel Otero-Pregigueiro[a], Ana Hernández-Pellón[a], Rafael Borge[b], Ignacio Fernández-Olmo[a]*

a Chemical and Biomolecular Engineering Department, University of Cantabria, Avda. Los Castros s/n, 39005 Santander, Cantabria, Spain

b Environmental Modelling Laboratory, Department of Chemical & Environmental Engineering, Technical University of Madrid, (UPM), 28006 Madrid, Spain.

*Corresponding Author

Chemical and Biomolecular Engineering Department, University of Cantabria, Avda. Los Castros s/n, 39005 Santander, Cantabria, Spain

fernandi@unican.es

ABSTRACT

Numerous studies have associated air manganese (Mn) exposure with negative health effects, primarily neurotoxic disorders. This work presents a description of the emission and dispersion of PM_{10}-bound Mn from industrial sources in the Santander bay area, Northern Spain. A detailed day-specific emission estimation was made and assessed for the main Mn source, a manganese alloy production plant under 8 different scenarios. Dispersion analysis of PM_{10}-bound Mn was performed using the CALPUFF model. The model was validated from an observation dataset including 101 daily samples from four sites located in the vicinities of the manganese alloy plant. Model results were in reasonable agreement with observations (r = 0.37; NMSE = 2.08; Fractional Bias = 0.44 and Modelled/Observed ratio = 1.57). Simulated and observed Mn concentrations in the study area were much higher than the guidelines proposed by the World Health Organization (WHO) and the U.S. Environmental Protection Agency (USEPA), highlighting the need to reduce the Mn concentrations in the area.

Based on the analysis of the Mn source contribution from the ferromanganese alloy plant, some preventive and corrective measures are discussed at the end of the paper. This work shows that CALPUFF dispersion model can be used to predict PM_{10}-bound Mn concentrations with reasonable accuracy in the vicinities of industrial facilities allowing the exposure assessment of the nearby population, which can be used in future epidemiological studies.

Keywords

Mn sources; ferromanganese alloy plant; CALPUFF; industrial emissions; air quality modelling

Highlights

A detailed Mn emission inventory for a ferromanganese alloy plant was developed

PM_{10}-bound Mn concentrations were modelled using CALPUFF

Based on model performance metrics, a reasonable prediction of Mn concentrations is obtained

Modelled and observed Mn concentrations regularly exceed the USEPA RfC in the study area

Control of fugitive emissions may substantially reduce Mn concentrations

1. Introduction

Manganese (Mn) is an essential trace element required for normal growth, development and cellular homeostasis (Erikson *et al.*, 2005). In humans and animals, Mn is required as a cofactor of several enzymes necessary for neuronal and glial cell function, as well as enzymes involved in neurotransmitter synthesis and metabolism (Erikson and Aschner, 2003). Nonetheless, excessive and prolonged inhalation of Mn particles results in its accumulation in selected brain regions that causes central nervous system dysfunctions and an extrapyramidal motor disorder, referred to as manganism (Park, 2013; Kwakye *et al.,* 2015). It is well known that occupational exposure to Mn can affect neuropsychological function (Finley, 2004). Several authors have pointed that the most hazardous route of Mn exposure is airborne. Inhaled Mn may enter the central nervous system (CNS) directly and be absorbed very effectively (Andersen *et al*., 1999; Krachler *et al*., 1999; Mergler *et al.*, 1999).

Studies regarding environmental air Mn exposure effects have been done, especially in susceptible groups like children (Crossgrove and Zheng, 2004; Riojas-Rodríguez *et al.*, 2010; Rodríguez-Barranco *et al.*, 2013; Carvalho *et al.*, 2014). Such studies suggest that environmental air Mn exposure may also be associated with neurotoxic disorders, including motor and cognitive deficits (Haynes *et al.,* 2010; Lucchini *et al.,* 2012; Roels *et al.,* 2012; Carvalho *et al.,* 2014; Chen *et al.,* 2016b; Menezes-Filho *et al.,* 2016). Due to the evidence of negative health effects as a consequence of environmental Mn overexposure, the World Health Organization (WHO) has proposed an annual average guideline value of 150 ng/m^3 (WHO, 2000). The U.S. Environmental Protection Agency (USEPA) has also proposed a daily reference concentration (RfC) of 50 ng/m^3 in the respirable fraction (US EPA, 1993). However, there is no specific European regulation that establishes airborne limit values for Mn.

Globally, 90 % of atmospheric Mn emissions are derived from natural sources (dust, erosion, volcanoes, sea-salt spray, etc.); however, in industrialized regions, anthropogenic emissions of Mn may explain the majority of atmospheric Mn inputs (Nriagu, 1989). High concentrations of Mn in air have been commonly associated with an industrial origin, such as Mn alloy and steel production, battery manufacturing and

Mn ore mining (Crossgrove and Zheng, 2004). High Mn concentrations in air have been widely reported in areas close to ferromanganese alloy plants, pointing out that even when PM_{10} concentrations fulfil the European regulatory limits, Mn should be a cause for concern in locations influenced by the emission from this activity. For instance, Colledge *et al.* (2015) reported a 24-h concentration of Mn of 1,130 ng/m^3 near of a ferromanganese refinery located in the Marietta community (Ohio, USA). Approximately 7.2 km to the north of this plant, in the city of Marietta (14,515 inhabitants), Haynes *et al.* (2010) reported an annual average concentration of 203 ng/m^3. Also, a 12-h average air Mn concentration of 7,560 ng/m^3 has been reported by Ledoux *et al.* (2006) in the vicinities of a ferromanganese plant located in Boulogne-Sur-Mer agglomeration (120,000 inhabitants, France). In the metropolitan area of Salvador (Brazil), 1.3 km from a ferromanganese alloy production plant, Menezes-Filho *et al.* (2009) reported a mean 24-h concentration of Mn in $PM_{2.5}$ of 151 ng/m^3. Other studies in the vicinity of closed manganese alloy production plants also reported elevated concentrations of Mn: 3,500 ng/m^3 (2-h) in Beauharnois, Canada (Boudissa *et al.*, 2006) and 49.5 ng/m^3(24-h) in Valcamonica, Italy (Lucchini *et al.*, 2012).

Airborne Mn concentrations of 4 – 23 ng/m^3 have been reported in several urban background sites in Spain (Querol *et al.*, 2007) although higher concentrations were measured at urban-industrial sites. For example, Querol *et al.* (2008) reported a concentration peak of 87 ng/m^3 close to a steel plant in Llodio (northern Spain) for the 1995-2005 period. Moreover, annual average concentrations above the WHO guidelines have been frequently reported in the vicinities of a manganese alloy plant in the Region of Cantabria, northern Spain (Figure 1). An annual average concentration of 166 ng/m^3 was reported in 2007 (Moreno *et al.*, 2011). Furthermore, annual average concentrations of 781 and 1,072 ng /m^3 were reported in 2005 and 2009 respectively, in the area of Maliaño, a small town where this ferroalloy plant is placed (CIMA, 2006; 2010). The application of corrective measures in the facility in 2008 led to an improvement in Mn air concentrations in Santander, where annual mean concentrations of 49.1 ng/m^3 (Arruti *et al.*, 2010) and 31.5 ng/m^3 (Ruiz *et al.*, 2014) were reported for 2008 and 2009, respectively. However, according to recent measurements, Mn concentrations in 2015 still exceeded the WHO recommendation in some areas of Maliaño, with monthly mean concentrations of 713.9 ng/m^3 and a maximum daily value of 3,200 ng/m^3 (Hernández-Pellón and Fernández-Olmo, 2016).

A common approach for assessing the exposure to Mn in the atmosphere is the measurement of the particulate matter-bound Mn concentration (Ledoux *et al.*, 2006; Moreno *et al.*, 2011; Marris *et al.*, 2012, 2013; Hernández-Pellón *et al.*, 2017). However, measurements are expensive, mainly for micropollutants such as trace metals, and may have limited spatial representativeness. Therefore, a combination of measurements and modelling approaches is desired in order to provide an integrated understanding of the phenomena and the assessment of population exposure (Chen *et al.*, 2012). In addition, dispersion model results are an essential instrument in the design and implementation of corrective measures.

The concentrations of several heavy metals have been modelled using different air quality models such as the Hybrid Single Particle Lagrangian Integrated Trajectory Model (HYSPLIT) for Cu, As, Zn, Co, Ni, Cr(Chen *et al.*, 2012, 2013, 2016a); Fine Resolution Atmospheric Multi-pollutant Exchange (FRAME) for As, Cr, Cd, Cu, Ni, Pb, Se, V, Zn(Dore *et al.*, 2014); CHIMERE Model for Pb, Cd, Ni, As, Cr, Se (González *et al.*, 2012); The Flexible Air Quality Regional Model (FARM) for Pb, Ni, Cd, As (Adani *et al.*, 2015); Community Multi-scale Air Quality (CMAQ) for Hg (Zhu *et al.*, 2015); CALPUFF Modeling System (CALPUFF) for Cd, Pb, Zn (MacIntosh *et al.*, 2010); AERMOD/CALPUFF Modeling Systems (AERMOD/CALPUFF) for Cr (Burger, 2004). However, few air manganese modelling studies have been done. Even though Haynes *et al.* (2010) modelled the exposure to Mn air concentrations through the AERMOD model and evaluated the relationship between biological measures of Mn in blood and hair, model outputs were not compared with observations. Carter *et al.* (2015) quantified integrated mass fluxes of Mn into soils and compared these soil-derived values with atmospheric deposition using the SCIPUFF model. Colledge *et al.* (2015) tried to assess airborne Mn concentration levels predicted by AERMOD by comparison with measurements. Nevertheless, Mn emission rates were derived from a simplified “site-surface area emission method” due to the difficulty of obtaining reliable emission data from the industries.

The aim of this study is to estimate the air Mn concentration in an urban area in the vicinity of a ferromanganese alloy plant using the CALPUFF dispersion model. In addition, the development of a detailed Mn emission inventory for the main source is done, which allows us to perform the simulation with a detailed day-by-day Mn emissions rate. Besides describing concentration patterns under different emission scenarios, the simulation is assessed by means of a multi-site dataset of PM_{10}-bound Mn concentrations from a previous 13 months experimental campaign.

2. Methodology

2.1. Site description

The area of study is located in the Region of Cantabria, along the Santander Bay in northern Spain (Figure 1). Terrain is relatively complex with a 600 m height mountain at 5km south, as well as a water mass in the bay. Main land uses are residential, industrial and commercial. SW and NE are the prevailing wind directions, as the wind rose plotted in Figure 1 shows.

This study focuses on Maliaño, a town of 10,000 inhabitants, located 7 km away from Santander City, where high concentrations of Mn in ambient air have been previously reported (Hernández-Pellón and Fernández-Olmo, 2016; Hernández-Pellón *et al.*, 2017).

The main Mn source in the area of study is a 225,000 t/year capacity ferromanganese alloy production plant. This plant, with a total operation area of 174,353 m^2, includes four electric arc furnaces, which are dedicated to high carbon ferromanganese (FeMn HC) and silicomanganese (SiMn), and an additional furnace is used to produce refined ferromanganese (FeMn MC). This factory has been operating since 1963 and is one of the most important ferroalloy plants in the world in terms of production capacity; even though the production went down during the economic crisis (42,000 tons in 2009), in the last years activity levels are similar to those reported before the crisis (131,000 tons in 2015). Three more factories have been identified as Mn sources in the area (Figure 1): a steel plant and two iron foundries that use Mn alloys as additives in their production processes although their Mn emissions are low according to the estimation described below.

2.2. Observations dataset

The observation dataset used in this paper was obtained from a 1 year 24-h PM_{10} sampling campaign from January 2015 to January 2016 that was carried out in the south of Santander bay (Hernández-Pellón and Fernández-Olmo, 2016). Sampling and analysis procedures are described in Hernández-Pellón and Fernández-Olmo (2016). The whole campaign includes 360 Mn daily values taken at nine sampling points throughout the area of interest. For this study, four representative sites close to the main manganese source were chosen (see Figure 1). At these four sites, 157 samples were available for the year 2015. From those, 101 samples had Mn concentrations above the USEPA RfC, i.e. 50 ng/m^3. Table 1 shows the statistics of all the observed PM_{10} - bound Mn concentrations at the selected four sites and the comparison after removing samples with concentrations lower than 50 ng/m^3.

2.3. Mn sources and estimated emissions

Manganese emissions from the main industrial sources in Santander bay were estimated. All point and area (fugitive) Mn sources were individually considered in this modelling assessment and are shown in Table 2. It was assumed that all manganese emissions are PM_{10} – bound (Carter *et al.*, 2015), with the exception of fugitive particle emissions from piles. In the later case, Mn emissions are assumed to be associated with total suspended particulates (TSP) considering a PM_{10}/TSP ratio of 0.5 (US EPA, 1998). Mn emissions were calculated by using emission factors obtained from US EPA (1984), and are expressed as kg/ton of product or kg /MWh (Table S1). Information about production rates, energy and raw material consumption, efficiency, and plant characteristics has been taken from Environmental Declarations of the companies (Ferroatlántica S.L., 2015; Global Steel Wire S.A., 2015) and Integrated Prevention and Pollution Control (IPPC) permits (BOC, 2008a, 2008b, 2008c, 2008d).

2.3.1. Emissions from the ferromanganese alloy plant

The refinery located in Maliaño specializes in ferromanganese (FeMn) and silicomanganese (SiMn) alloy production. Four electric arc furnaces (20 MW, 30 MW and 2x35 MW) are dedicated equally to FeMn HC and SiMn, and an additional 3 MW furnace is used for FeMn MC production. The production of these alloys releases Mnbearing particles in different sections of the production process. Figure 2 sumarizes the main point and fugitive sources of air Mn associated to this process.

Point sources may be systematic and non-systematic. The systematic point sources work under regular operation conditions. They include: (i) Flare emissions: the off-gas exiting the electric arc furnace is filtered by a wet scrubber before it is flared-out. The manganese emissions depend on the amount of particles generated in the furnace and on the scrubber efficiency. Four point sources corresponding to the four furnaces have been considered. (ii) Controlled stack emissions from tapping/ladle/casting: fugitive particle emissions from tapping, ladle and casting are hooded and filtered by a baghouse. Two point sources corresponding to the exit of the baghouses of the two smelting buildings have been considered. (iii) Controlled stack emissions from FeMn MC manufacture: emissions produced in the FeMn MC furnace are filtered by a baghouse. One point source corresponding to this furnace has been considered. (iv) Controlled stack emissions from product handling and processing: once the ferroalloys are obtained they are subjected to handling, grinding, classification and trucks loading. Fugitive particle emissions are also hooded and filtered by baghouses. Five point sources have been considered for these operations. Non-systematic point sources correspond to the alternative bypass of the off-gas control equipment to reduce the risk of fire or explosion under certain operation conditions. Four non-systematic point sources corresponding to the four main furnaces have been considered. The different types of point sources considered in this study are shown in Table 2.

Main fugitive sources are uncontrolled smelting emissions, and ores and slag pile emissions: (i) Uncontrolled smelting emissions are produced in tapping, ladle and casting operations when particles are not fully captured by the hooding system; these emissions are generated inside the buildings and are emitted through the openings located in the building walls. These emissions are defined as two volume sources corresponding to the two furnace/ladle buildings. (ii) Ores and slag pile emissions consist of manganese-bearing particles released by wind erosion and handling. These emissions are defined as area sources; three areas are considered based on the piles location. The selected fugitives sources are also summarized in Table 2.

Daily production rates and the operation hours of each furnace have been used to calculate a detailed hourly emission inventory for the plant. Hourly wind data from a local meteorological station located in Guarnizo (500 meters south of the ferromanganese alloy plant), have been used to calculate TSP fugitive emissions from piles, according to the procedure given in Section 11.9 of US EPA (1988). Even though this method does not include pluviometry in its calculation, it was used because of its simplicity and the low frequency (8% during the period of interest) of high precipitation events. It is assumed that during rain events Mn concentrations may be slightly overestimated, since it is known that rainfall diminishes dust fugitive emissions from piles. A PM_{10}/TSP ratio of 0.5 and a Mn content of 45 % were applied to estimate the PM_{10}-bound Mn emission rate (US EPA, 1998). Therefore, an hourly Mn emission rate for every source and for every day of the studied period has been calculated to feed the dispersion model.

2.3.2. Emissions from other industrial sources

Emission rate calculations from other industrial sources have been simplified because of the low contribution to the total Mn emissions as they do not use Mn as a main product in their productive process. A single point source is considered for each of the following plants (see Table 2): (i) Steel plant: stack emissions from the electric arc furnace filtered by a baghouse before releasing. (ii) Iron foundry 1: stack emissions from the cupola furnaces treated by a baghouse. (iii) Iron foundry 2: stack emissions generated in the cupola furnaces treated by a wet scrubber. A constant emission rate for the whole year was assumed for these industrial sources.

2.4. Air quality modelling system and model set-up

CALPUFF is a multi-layer, multi-species non-steady-state Lagrangian puff dispersion model which can simulate the effects of time and space-varying meteorological conditions on pollutant transport, transformation, and removal (Scire *et al.*, 2000). The model has been adopted by the USEPA in its *Guideline on Air Quality Models* as a preferred model. The integrated modelling system consists of three main components that are CALMET (a diagnostic 3 – dimensional meteorological model), CALPUFF (an air quality dispersion model), and CALPOST (a postprocessing package). In this study, the

USEPA approved version of CALPUFF (v5.8) included in CALPUFF View interface (v8.4.0) has been used.

A grid domain of 20 km x 20 km with 10,000 cells of 200 m x 200 m each was used; the center of the grid is defined by the location of the ferromanganese alloy plant. Terrain elevation has been obtained from the Shuttle Radar Topography Mission (SRTM 1) with a resolution of 90 m. Land cover data have been obtained from the Global Land Cover Characterization (GLCC) with 1 km spatial resolution. Meteorological information necessary to run CALMET has been taken from local meteorological stations. 1-hour resolution surface data from three locations (Parayas AEMET X: 432703 m Y: 4808800 m; Santander-CMT AEMET X: 435281 m Y: 4815665 m and Guarnizo CIMA X: 432146 m Y: 4806368 m, Figure 1) have been combined with representative upper air data from vertical soundings at Santander-CMT meteorological station.

Dry and wet deposition were also evaluated, considering a mean particle diameter of 0.84 µm with a standard deviation of 0.47 µm. These values were obtained from Hernández-Pellón *et al.* (2017), who measured the particle size of manganese-bearing particles contained in PM_{10} filters collected in the area of study. Scavenging Coefficient for the liquid precipitation was calculated according to Jindal and Heinold (1991). The model has been run with the "puff" option as it produces similar model results but involves significantly shorter run times than the "slug" approach.

2.5. Model performance evaluation and sensitivity analysis to different emission scenarios

CALPUFF was run for 101 days in 2015, corresponding to daily samples having Mn concentrations above the USEPA RfC, i.e. 50 ng/m^3, to improve our understanding of the conditions that yielded higher concentrations and the associated exposure levels. A set of descriptive statistics, including standard deviation, mean, and median were generated to compare measured and modelled PM_{10} - bound Mn data for each receptor. Model performance was assessed through a series of common statistics (Thunis *et al.*, 2012): Pearson Correlation Coefficient (r), normalized-mean-square error (NMSE), Fractional Bias (FB) and Modelled – Observed ratio (Mod/Obs). Taylor Diagram (Taylor, 2001) is also included in the analysis since it conveys information of three complementary model performance statistics simultaneously on a single 2D graph: correlation coefficient, standard deviation and root-mean-square error (RMS).

A preliminary study to evaluate model sensitivity to uncertain emission input data was performed. These were the hooding efficiency in the smelting furnace buildings, and the area and height of Mn ore piles. Since ore pile height and area change over time, a high uncertainty is associated with these sources. Thus, an area of 4,269 m^2, corresponding to the total available open storage surface, and a 50% of this area, 2,134 m^2, were selected. In addition, two pile heights (8 and 16 meters) were proposed, based on in-situ observations. According to the Best Available Techniques Reference Document for the Non-Ferrous Metals Industries (European Commission, 2014), hooding efficiencies of 96 % and 86% have been proposed since the exact collection efficiency in this particular plant is not known. Therefore, eight different emission scenarios were defined (see Table 3) to study the influence of these inputs on modelled PM_{10}-bound manganese surface concentrations. This information is useful for identifying the relevant scale of the dispersion processes, the location of highest concentration areas and the spatial variability of airborne Mn within the modelling domain.

3. Results and discussion

3.1. Model performance by emission scenario

Model outputs were compared with observations to provide an estimate of the modelling system capabilities to reproduce measurements and to gain a better understanding regarding likely values of some highly uncertain emission parameters. Table 4 shows the performance metrics used to compare the CALPUFF model predictions with the measured concentrations for each of the scenarios simulated (Table 3). Statistically significant correlations (r-values) for 95% confidence level were found for 6 of the 8 scenarios modelled, ranging from 0.19 to 0.42 (S1). These values are similar to those obtained by Chen *et al.* (2013) for different metals in the Algeciras Bay industrial area, which varied from 0.13 to 0.39.

NMSE values varied from 1.99 to 8.26, with lower values associated with scenarios where hooding efficiency was 96% (S1 to S4). Fractional Bias values varied from 0.15 to 1.24, showing a systematic overestimation in all the scenarios, mainly for those considering a 86 % hooding efficiency (S5 to S8). Nonetheless, these values fall within the ranges proposed by Borrego *et al.* (2008) of (-2) – 2. Kumar *et al.* (2006) proposed a more restrictive range of (-0.5) – 0.5, which is only met by S2, S3 and S4 scenarios. This range is often acceptable for major pollutants, but it is rarely used for metals. The ratio between modelled and observed concentrations (Mod/Obs) varied from 1.16 to 4.27. Colledge *et al.* (2015) reported modelled/observed ratios for TSP air-Mn from 0.54 to 5.17 in two residential areas close to industrial Mn sources in Ohio, USA. Tartakovsky *et al.* (2013) obtained worse concentration ratios for TSP that varied from 0.04 to 0.34. Even though the Mod/Obs scores from this study are better, only the results for the S2, S3 and S4 scenarios would be within the proposed acceptable range of 0.5 – 2 suggested by Borrego et al. (2008).

This analysis points out that hooding efficiency is the most influential variable, since a moderate change of this parameter (from 96 to 86 %) leads to a large increase in Mn concentrations. Although piles surface area only affects fugitive emissions from ore/slag handling and storage, a moderate effect on the Mn modelled concentrations is observed as well. The results point out that for the same pile height, 50% pile surface scenarios yielded better results (in terms of NMSE, FB and Mod/Obs ratios) than those considering 100% pile surface. In situ and aerial observations of piles confirm that both, pile surface area and height keep changing in time leading to different particulate matter emission patterns. Therefore, a 50 % piles surface area was assumed as a reasonable compromise for modelling purposes. Finally, pile height was found to have a lower impact on model performance. While 8 meters pile height odd scenarios showed higher correlation coefficients, the other performance statistics were worse than those scenarios that considered a 16 meters pile height. In particular, 8 meters pile-scenarios lead to an overestimation of Mn concentrations in the closest site (CCV), but capture better the variability of daily Mn concentrations, leading to higher correlation coefficients. To provide a complementary view of model performance by scenario, a Taylor diagram was also plotted (Figure S1). This analysis confirmed that S1 to S4 scenarios showed a better performance. Eventually S2, S3 and S4 were selected since they provide a good compromise between relatively low RMS error and high correlation factor.

3.2. Model performance by site

Once overall performance was assessed considering all samples and locations, a site-specific analysis was made based on the emission scenarios that best reproduced the observations according to the discussion in the previous section.

Table 5 shows the performance metrics computed for each monitoring site (S2, S3 and S4 scenarios). NMSE, FB and Mod/Obs concentrations are particularly good in CROS and CMFC for the three scenarios while in CCV, only 350 meters north from the manganese alloy plant, metric values were slightly worse. Despite presenting larger overestimations and general poorer performance, GUAR showed the highest correlation comparatively with the rest of the sites. This overestimation may be due to the proximity of the receptor site to the main Mn sources (600 m south) but it may be affected also by the small number of samples available at this site (11).

Table 6 shows a comparison between PM_{10}-bound observed and modelled Mn concentrations for all the studied sites. The arithmetic mean of simulated PM_{10}-bound Mn concentrations was 762 ng/m^3 in S2, 826 ng/m^3 in S3 and 611 ng/m^3 in S4, while the mean observed concentration was 527 ng/m^3. Figure 3 compares observed and predicted Mn through scenario-specific scatterplots. The clouds of points are in reasonable proximity to the 1:1 slope with the exception of some few values in CROS site. The results show a larger spread for this location indicating that observations at this site may be affected to a larger extent by very local dispersion phenomena induced by the urban canopy. Although land uses in the vicinities of the plant are similar and the four locations selected meet similar criteria in terms of avoiding small scale dispersion phenomena, the CROS monitoring site is surrounded by a more complex urban geometry (as can be seen in Figure 1) and thus local dispersion may be more influenced by building wakes and shielding effects.

The temporal trends of observed and modelled Mn concentrations (for S2 to S4 scenarios) at each receptor are compared in Figure 4. The model is able to capture the underlying trend although deviations are not systematic and may be considerably high for specific days. The accuracy of the model could be improved with the experimental determination of the PM_{10}/TSP ratio and percentage of Mn in particles collected around the ores pile area together with the particle size distribution at the point sources of the manganese alloy plant. The use of a high-resolution Weather Research and Forecasting (WRF) modeling system to produce meteorological data has improved the accuracy of the prediction of metal concentrations in some dispersion modeling studies (e.g. Chen *et al.,* 2016a); however, in the present study the quality of the observed meteorological data is good enough to describe reasonably well the dispersion of Mn in the studied area.

3.3. Mn environmental exposure assessment

The previous results may support the choice of S3 as the best modelling scenario. While having good statistics, similar to S2 and S4, it exhibits a better correlation. Arithmetic means for the whole simulated period (101 days, S3 scenario) are 1,738 ng/m^3 in CCV; 519 ng/m^3 in GUAR; 465 ng/m^3 in CROS and 594 ng/m^3 in CMFC. This clearly reflects that most of the modelled daily PM_{10}-bound Mn concentrations in Maliaño are much higher than the USEPA RfC (50 ng/m^3). According to CALPUFF simulated surface maps, the maximum PM_{10}-bound Mn concentration levels are located in the surrounding area of the ferromanganese alloy plant, with daily average concentration levels up to 5,000 ng/m^3 in Maliaño (under moderate intensity south-west wind conditions). However, the model indicates that Mn plumes are dispersed along the Santander bay turning out in concentration levels around 200 ng/m^3 in the city, which is the most populated area in the region (172,656 inhabitants in 2016). Three events under SW and W wind directions corresponding to 06/26/2015 (Figure 5a), 09/13/2015 (Figure 5b) and 11/13/2015 (Figure 5c) illustrate this situation. Since SW is the prevailing wind direction in the area, the plume was similar in several modelled days, resulting in higher PM_{10}-bound Mn concentrations in the receptors located to the north of the ferromanganese alloy plant, especially in the closest one: CCV (Figure 1). According to the simulation performed, the steel plant, iron foundry 1 and iron foundry 2 have minimal effects on the PM_{10}-bound Mn concentration in the study area, especially in comparison with the manganese alloy plant, which is the main contributor to the high Mn concentrations in the study area.

3.4. Potential preventive and corrective measures

The contribution of the studied plants to the total Mn emission was assessed. Under the conditions given by S3 scenario, the ferromanganese alloy plant accounted for 91% of the total Mn emissions within the modelling domain; the contribution of the iron foundry #2, the steel plant and the iron foundry #1 were 4%, 3%, and 2%, respectively. Because the ferroalloy plant was the main Mn emitter, the different Mn sources within this plant were evaluated to identify the highest emission sources and thus, potential preventive and corrective measures useful to decrease Mn concentration in the area. Fugitive sources accounted for 72% of the total Mn emissions (66 % from furnace buildings and 6 % from ore/slag piles). The importance of fugitive emissions from Mn alloys manufacturing has been previously highlighted in the literature. According to Carter *et al.* (2015), up to 65 % of air Mn emissions from a FeMn plant located in Marietta (Ohio) were attributed to fugitive sources. Davourie *et al.* (2017) also reported that material handling originates the 35 % of PM emissions. Moreover, secondary emissions dispersed during tapping and casting are not fully controlled using fume hood and baghouse systems, leading to additional fugitive emissions in furnace operation. The analysis of Mn emissions from S3 scenario also shows that 30 % of the point source emissions were produced by non-systematic sources, even though they only operate for short periods. This is in agreement with Davourie *et al*. (2017), that also reported that despite short durations operating with by-pass flaring or venting, uncontrolled emissions comprise over 36% of PM emitted from manganese furnaces.

These results point out that some strategies to reduce Mn concentration in residential areas near the ferromanganese alloy plant are as follows: (i) to improve the hooding efficiency in furnace buildings; (ii) to reduce the fugitive emissions from ore/slag storage and handling; (iii) to better regulate the furnace operation to reduce abnormal operating conditions, and to install the same control devices for particulate matter in the by-pass pipeline. Although the existing secondary fume capture system has good capacity, fugitive emissions from the furnace building do occur and the optimization and upgrading of the capture system are recommended (Els *et al.*, 2013). In addition, three open storage areas for Mn ores and slags still remain in the plant.

4. Conclusions

The CALPUFF dispersion model was used to simulate PM_{10}-bound Mn concentrations in the Santander bay, Northern Spain, where different Mn industrial sources are located. An exhaustive operation analysis of a ferromanganese alloy plant was done, which allowed us to develop a detailed day-by-day Mn emission inventory, including point and fugitive sources.

The model reproduced observed PM_{10}-bound Mn concentrations in the study area for different emission scenarios with reasonable accuracy. A strong concentration gradient is predicted, agreeing well with the observation profile. However, possible options for future improvements may include the initialization of CALPUFF from high-resolution mesoscale meteorological simulations and the refinement of the emission inventory by incorporating detailed particle size distribution for each emission source as well as precise plant operation patterns.

Modelled and observed Mn average concentrations in Maliaño exceed the reference concentration proposed by the USEPA (i.e. 50 ng/m^3). This can be exceeded even in Santander City when SW wind events occur according to the model. This modelling assessment confirms the need for reducing Mn airborne concentrations in the Santander bay. The high spatial variability of the Mn concentration patterns predicted in the vicinities of the Maliaño manganese alloy plant suggests that the use of these kinds of models may be key for the design and assessment of future epidemiological studies both in the area of study and elsewhere. Preventive and corrective measures based on the removal of fugitive and non-systematic point source emissions may be implemented to effectively reduce the Mn environmental exposure to the population affected by such plants.

Acknowledgments

This work was supported by the Spanish Ministry of Economy and Competitiveness (MINECO) through the Project CTM2013-43904R. The authors also acknowledge the

Spanish State Meteorology Agency (AEMET) for providing meteorological and atmospheric sounding data for the period of study.

REFERENCES

Adani, M., Mircea, M., D'Isidoro, M., Costa, M.P., Silibello, C. (2015) *Heavy metal modelling study over Italy: Effects of grid resolution, lateral boundary conditions and foreign emissions on air concentrations*, Water, Air, and Soil Pollution, 226(3).

Andersen, M., Gearhart, J. and Clewell, H. (1999) *Pharmacokinetic data needs to support risk assessments for inhaled and ingested manganese*, NeuroToxicology, 20(2–3), 161–171.

Arruti, A., Fernández-Olmo, I. and Irabien, Á. (2010) *Evaluation of the contribution of local sources to trace metals levels in urban PM2.5 and PM10 in the Cantabria region (Northern Spain)*, Journal of Environmental Monitoring, 12(7), 1451.

BOC (2008a) *Autorización Ambiental Integrada: Ferroatlántica S.L.*, Boletín Oficial Cantabria 107. 7569-7582

BOC (2008b) *Autorización Ambiental Integrada: Global Steel Wire S.A.*, Boletín Oficial Cantabria, 125, 8967–8977.

BOC (2008c) *Autorización Ambiental Integrada: Industrias Hergom S.A.,* Boletín Oficial Cantabria, 248, 17477–17488.

BOC (2008d) *Autorización Ambiental Integrada: Saint-Gobain Canalización S.A.,* Boletín Oficial Cantabria, 142, 9965-9974.

Borrego, C., Monteiro, A., Ferreira, J., Miranda, A.I., Costa, A.M., Carvalho, A.C., Lopes, M. (2008) *Procedures for estimation of modelling uncertainty in air quality assessment,* Environment International 34, 613–620.

Boudissa, S.M., Lambert, J., Muller, C., Kennedy, G., Gareau, L., Zayed, J. (2006) *Manganese concentrations in the soil and air in the vicinity of a closed manganese alloy production plant*, Science of the Total Environment, 361(1–3), 67–72.

Burger, L. W. (2004) *Hexavalent Chromium Air Dispersion Modelling in the South African Ferrochromium Industry,* Control, 806–817.

Carter, M.R., Gaudet, B.J., Stauffer, D.R., White, T.S., Brantley, S.L.(2015) *Using soil records with atmospheric dispersion modeling to investigate the effects of clean air regulations on 60 years of manganese deposition in Marietta, Ohio (USA),* Science of the Total Environment., 515–516, 49–59.

Carvalho, C.F., Menezes-Filho, J.A., de Matos, V.P., Bessa, J.R., Coelho-Santos, J., Viana, G.F.S., Argollo, N., Abreu, N. (2014) *Elevated airborne manganese and low executive function in school-aged children in Brazil,* NeuroToxicology, 45, 301–308.

Chen, B., Stein, A.F., Castell, N., de la Rosa, J. D., Sanchez de la Campa, A.M., Gonzalez-Castanedo, Y., Draxler, R.R. (2012) *Modeling and surface observations of arsenic dispersion from a large Cu-smelter in southwestern Europe,* Atmospheric Environment. 49, 114–122.

Chen, B., Stein, A.F., Guerrero Maldonado, P., Sanchez de la Campa, A.M., Gonzalez-Castanedo, Y., Castell, N., de la Rosa, J.D. (2013) *Size distribution and concentrations of heavy metals in atmospheric aerosols originating from industrial emissions as predicted by the HYSPLIT model,* Atmospheric Environment., 71, 234–244.

Chen, B., Stein, A.F., Castell, N., Gonzalez-Castanedo, Y., Sanchez de la Campa, A.M., de la Rosa, J.D.(2016a) *Modeling and evaluation of urban pollution events of atmospheric heavy metals from a large Cu-smelter,* Science of the Total Environment, 539,17–25.

Chen, P., Culbreth, M. and Aschner, M. (2016b) *Exposure, epidemiology, and mechanism of the environmental toxicant manganese, Environmental Science and Pollution Research.* Environmental Science and Pollution Research, 23(14), 13802–13810.

CIMA. Government of Cantabria, 2006. *Evaluación de la influencia de la dirección del viento en el manganeso contenido en la fracción PM10 en Alto Maliaño*. Internal Report C- 098/2004.4.

CIMA, Government of Cantabria, 2010. *Evaluación de la calidad del aire y analítica de metales en la fracción PM10 en el Alto Maliaño*. Internal Report C-077/2008.

Colledge, M. A., Julian, J.R., Gocheva, V.V., Beseler, C.L., Roels, H.A., Lobdell, D.T., Bowler, R.M. (2015) *Characterization of air manganese exposure estimates for* *residents in two Ohio towns*, Journal of the Air & Waste Management Association 28(10), 1304–1314.

Crossgrove, J. and Zheng, W. (2004) *Manganese toxicity upon overexposure, NMR* in Biomedicine*,* Wiley InterScience 17(8), 544–553.

Davourie, J., Westfall, L., Ali, M., McGough, D. (2017) *Evaluation of particulate matter emissions from manganese alloy production using life-cycle assessment,* NeuroToxicology. 58, 180–186.

Dore, A. J., Hallsworth, S., McDonald, A., Werner, M., Kryza, M., Abbot, J., Nemitz, E., Dore, C.J., Malcolm, H., Vieno, M., Reis, S., Fowler, D. (2014) *Quantifying missing annual emission sources of heavy metals in the United Kingdom with an atmospheric transport model,* Science of the Total Environment, 479–480(1), 171–180.

Els, L., Cowx, P., Nordhagen, R., Kornelius, G., Andrew, N., Smith, P. (2013) *Analysis of a ferromanganese secondary fume extraction system to improve design methodologies,* The thirteenth International Ferroalloys Congress, 967–978.

Erikson, K. M., Syversen, T., Aschner, J.L., Aschner, M. (2005*) Interactions between excessive manganese exposures and dietary iron-deficiency in neurodegeneration,* Environmental Toxicology and Pharmacology, 19(3), 415–421.

Erikson, K. M. and Aschner, M. (2003) *Manganese neurotoxicity and glutamate-GABA interaction,* Neurochemistry International, 43(4–5), 475–480.

European-Commission (2014) *Reference Document for the Non-Ferrous Metals Industries. Best Available Techniques (BAT)*. *http://eippcb.jrc.ec.europa.eu/reference/BREF/NFM_Final_Draft_10_2014.pdf*

Ferroatlántica S.L. (2015) *Declaración Ambiental 2015 Centro Productivo: Fábrica de Boo.*

Finley, J. W. (2004) *Does environmental exposure to manganese pose a health risk to healthy adults?,* Nutrition reviews, 62(4), 148–153.

Global Steel Wire S.A. (2015*) Declaración Ambiental GSW. http://www.globalsteelwire.com/Pdf/productos/DECLARACI%C3%93N%20AMBIENTAL%202015%201S2016.pdf*

González, M. Á., Vivanco, M.G., Palomino, I., Garrido, J.L., Santiago, M., Bessagnet, B. (2012) *Modelling some heavy metals air concentration in europe,* Water, Air, and Soil Pollution, 223(8), 5227–5242.

Haynes, E. N., Heckel, P., Ryan, P., Roda, S., Leung, Y.K., Sebastian, K., Succop, P. (2010) *Environmental manganese exposure in residents living near a ferromanganese refinery in Southeast Ohio: A pilot study,* NeuroToxicology. 31(5), 468–474.

Hernández-Pellón, A., Fernández-Olmo, I., Ledoux, F., Courcot, L., Courcot, D. (2017) *Characterization of manganese-bearing particles in the vicinities of a manganese alloy plant,* Chemosphere, 175, 411–424.

Hernández-Pellón, A., Fernández-Olmo, I. (2016). *Monitoring the levels of particle matter-bound manganese: An intensive campaign in an urban/industrial area.* Conference Proceedings 2nd International Conference on Atmospheric Dust - DUST2016. ProScience 3, 50-55.

Jindal, M., Heinold, D. (1991). *Development of particulate scavenging coefficients to model wet deposition from industrial combustion sources. Paper #91-59.7*, 84th annual meeting of the Air and Waste Management Assoc., Vancouver, BC, Canada, June 15-21.

Krachler, M., Rossipal, E. and Micetic-Turk, D. (1999) *Concentrations of trace elements in sera of newborns, young infants, and adults.,* Biological trace element research, 68(2), 121–35.

Kumar, A., Dixit, S., Varadarajan, C., Vijayan, A., Masuraha, A. (2006) *Evaluation of the AERMOD Dispersion Model as a Function of Atmospheric Stability for an Urban Area,* Wiley InterScience 25(2), 141–151.

Kwakye, G. F., Paoliello, M.M.B., Mukhopadhyay, S., Bowman, A., Aschner, M. (2015) *Manganese-induced parkinsonism and Parkinson's disease: Shared and distinguishable* *features,* International Journal of Environmental Research and Public Health, 12(7), 7519–7540.

Ledoux, F., Laversin, H., Courcot, D., Courcot, L., Zhilinskaya, E.A., Puskaric, E., Aboukaïs, A. (2006) *Characterization of iron and manganese species in atmospheric aerosols from anthropogenic sources,* Atmospheric Research, 82(3–4), 622–632.

Lucchini, R. G., Guazzetti, S., Zoni, S., Donna, F., Peter, S., Zacco, A., Salmistraro, M., Bontempi, E., Zimmerman, N.J., Smith, D.R. (2012) *Tremor, olfactory and motor changes in Italian adolescents exposed to historical ferro-manganese emission,* NeuroToxicology, 33(4), 687–696.

MacIntosh, D. L., Stewart, J.H., Myatt, T.A., Sabato, J.E., Flowers, G.C., Brown, K.W., Hlinka, D.J., Sullivan, D.A. (2010) *Use of CALPUFF for exposure assessment in a near-field, complex terrain setting,* Atmospheric Environment., 44(2), 262–270.

Marris, H., Deboudt, K., Augustin, P., Flament, P., Blond, F., Fiani, E., Fourmentin, M., Delbarre, H. (2012) *Fast changes in chemical composition and size distribution of fine particles during the near-field transport of industrial plumes,* Science of the Total Environment., 427–428, 126–138.

Marris, H., Deboudt, K., Flament, P., Grobéty, B., Gieré, R. (2013) *Fe and Mn oxidation states by TEM-EELS in fine-particle emissions from a Fe-Mn alloy making plant,* Environmental Science and Technology, 47(19), 10832–10840.

Menezes-Filho, J. A., Paes, C.R., de C. Pontes, Â.M., Moreira, J.C., Sarcinelli, P.N., Mergler, D. (2009) *High levels of hair manganese in children living in the vicinity of a ferro-manganese alloy production plant*, NeuroToxicology, 30(6), 1207–1213.

Menezes-Filho, J. A., Fraga de Souza, K.O., Gomes Rodrigues, J.L., Ribeiro dos Santos, N., De Jesus Bandeira, M., Koin N.L., do Prado Oliveira, S.S., Campos Godoy, A.L.P., Mergler, D. (2016*) Manganese and lead in dust fall accumulation in elementary schools near a ferromanganese alloy plant,* Environmental Research, 148, 322–329.

Mergler, D., Baldwin, M., Bélanger, S., Larribe, F., Beuter, A., Bowler, R., Panisset, M., Edwards, R., de Geoffroy, A., Sassine, M.P., Hudnell, K. (1999) *Manganese* *neurotoxicity, a continuum of dysfunction: Results from a community based study,* NeuroToxicology, 20(2–3), 327–342.

Moreno, T., Pandolfi, M., Querol, X., Lavín, J., Alastuey, A., Viana, M., Gibbons, W. (2011) *Manganese in the urban atmosphere: Identifying anomalous concentrations and sources,* Environmental Science and Pollution Research, 18(2), 173–183.

Nriagu, J. O. (1989) *A global assessment of natural sources of atmospheric trace metals,* Nature, 338 (6210), 47–49.

Park, R. M. (2013*) Neurobehavioral deficits and parkinsonism in occupations with manganese exposure: A review of methodological issues in the epidemiological literature,* Safety and Health at Work., 4(3), 123–135.

Querol, X., Viana, M., Alastuey, A., Amato, F., Moreno, T., Castillo, S., Pey, J., de la Rosa, J., Sánchez de la Campa, A., Arííñano, B., Salvador, P., García Dos Santos, S., Fernández-Patier, R., Moreno-Grau, S., Negral, L., Minguillón, M.C., Monfort, E., Gil, J.I., Inza, A., Ortega, L.A., Santamaría, J.M., Zabalza, J. (2007) *Source origin of trace elements in PM from regional background, urban and industrial sites of Spain,* Atmospheric Environment, 41(34), 7219–7231.

Querol, X., Alastuey, A., Moreno, T., Viana, M. M., Castillo, S., Pey, J., Rodríguez, S., Artiñano, B., Salvador, P., Sánchez, M., Garcia Dos Santos, S., Herce Garraleta, M.D., Fernandez-Patier, R., Moreno-Grau, S., Negral, L., Minguillón, M.C., Monfort, E., Sanz, M.J., Palomo-Marín, R., Pinilla-Gil, E., Cuevas, E., de la Rosa, J., Sánchez de la Campa, A. (2008) *Spatial and temporal variations in airborne particulate matter (PM10 and PM2.5) across Spain 1999–2005.* Atmospheric Environment, 42, 3964–3979.

Riojas-Rodríguez, H., Solís-Vivanco, R., Schilmann, A., Montes, S., Rodríguez, S., Ríos, C., Rodríguez-Agudelo, Y. (2010) *Intellectual function in Mexican children living in a mining area and environmentally exposed to manganese,* Environmental Health Perspectives, 118(10), 1465–1470.

Rodríguez-Barranco, M., Lacasaña, M., Aguilar-Garduño, C., Alguacil, J., Gil, F., González-Alzaga, B., Rojas-García, A. (2013) *Association of arsenic, cadmium and manganese exposure with neurodevelopment and behavioural disorders in children: A* *systematic review and meta-analysis,* Science of the Total Environment, 454–455, 562–577.

Roels, H. A., Bowler, R.M., Kim, Y., Henn, B.C., Mergler, D., Hoet, P., Gocheva, V.V., Bellinger, D.C., Wright, R.O., Harris, M.G., Chang, Y., Bouchard, M.F., Riojas-Rodriguez, H., Menezes-Filho, J.A., Téllez-Rojo, M.M. (2012) *Manganese exposure and cognitive deficits: A growing concern for manganese neurotoxicity*, NeuroToxicology, 33(4), 872–880.

Ruiz, S., Fernández-Olmo, I. and Irabien, Á. (2014) *Discussion on graphical methods to identify point sources from wind and particulate matter-bound metal data,* Urban Climate, 10, 671–681.

Scire, J. S., Strimaitis, D. G. and Yamartino, R. J. (2000) *A User ' s Guide for the CALPUFF Dispersion Model*. Earth Tech, Inc. http://www.src.com/calpuff/download/CALPUFF_UsersGuide.pdf

Tartakovsky, D., Broday, D. M. and Stern, E. (2013) *Evaluation of AERMOD and CALPUFF for predicting ambient concentrations of total suspended particulate matter (TSP) emissions from a quarry in complex terrain,* Environmental Pollution, 179, 138–145.

Taylor, K. E. (2001) *Summarizing multiple aspects of model performance in a single* diagram, J. Geophys. Res. Atmos, 106, 7183–7192.

Thunis, P., Georgieva, E., & Pederzoli, A. (2012) *A tool to evaluate air quality model performances in regulatory applications.* Environmental Modelling and Software, 38, 220–230.

US EPA (1984) *Locating and Estimating Sources of Manganese.* https://www3.epa.gov/ttnchie1/le/manganes.pdf

US EPA (1988) *AP 42: Control of open fugitive dust sources, Section 11.* https://www3.epa.gov/ttn/chief/old/ap42/ch13/s025/reference/ref_10c13s025_1995.pdf

US EPA (1993) *Printout of reference concentration (RfC) for chronic inhalation exposure for manganese as verified 9/23/93, dated 12/93.*

World Health Organization (2000) *Air Quality Guidelines for Europe.* WHO Regional Publications, European Series (91), 288.

Zhu, J., Wang, T., Bieser, J., Matthias, V. (2015) *Source attribution and process analysis for atmospheric mercury in eastern China simulated by CMAQ-Hg,* Atmospheric Chemistry and Physics, 15(15), 8767–8779.

TABLES

Table 1. Basic statistics of observed PM_{10}-bound Mn concentrations (24-h averages) from January 2015 to January 2016 (> USEPA RfC and overall campaign)

Receptor site	UTM (m)	Distance from alloy plant (m)	All samples (ng/m^3)					Samples > USEPA RfC[a] (ng/m^3)				
			n	Mean	Median	SD	Max	n	Mean	Median	SD	Max
CCV	X: 431899 Y: 4807290	440	27	695	467	651	2,062	23	813	813	635	2,062
CROS	X: 431916 Y: 4807982	1,130	75	260	87	369	1,670	44	390	198	411	1,670
CMFC	X: 432128 Y: 4808086	1,240	28	589	308	575	1,859	23	682	577	571	1,859
GUAR	X: 432146 Y: 4806368	690	27	156	52	227	917	11	314	203	249	917

[a] Values above the USEPA RfC, i.e. 50 ng/m^3.

Table 2. Mn sources and estimated emission rates.

Factory type	Source description	Production area	Source type	Number of sources [a]	Mn emission rate (gMn/day)[b]
Manganese alloy plant	Smelting flares	Smelting	Systematic point	4	1,772
	Refined furnace stack	Smelting	Systematic point	1	177
	Furnace buildings stacks	Tapping, ladle, casting	Systematic point	2	7,363-8,219
	Product processing stacks	Product handling, grinding, sieving	Systematic point	5	289
	Smelting by-pass stacks	Smelting	Non-systematic point	4	4,122
	Furnace buildings wall openings	Tapping, ladle, casting	Fugitive, volume	2	34,247-119,864
	Ore and slag piles	Mn ore and slag handling and storage	Fugitive, area	3	3,264-6,529
Steel plant	Furnace stack	Electric arc furnace	Systematic point	1	1,545
Iron foundry 1	Cupola stack	Cupola	Systematic point	1	1,112
Iron foundry 2	Cupola stack	Cupola	Systematic point	1	2,304

[a] For Steel plant, Iron foundry 1 and Iron foundry 2 a single point source was considered for each of the plants.

[b] Range of Mn emission rates for different scenarios

Table 3. Emission scenarios

Scenario	**Hooding Efficiency (%)**	**Pile area (m^2)**	**Pile Height (m)**
S1	96	4,269	8
S2	96	4,269	16
S3	96	2,134	8
S4	96	2,134	16
S5	86	4,269	8
S6	86	4,269	16
S7	86	2,134	8
S8	86	2,134	16

Table 4. Statistics obtained from the comparison between observed and simulated PM_{10}-bound Mn concentration values for each emission scenario (dimensionless): r (correlation coefficient); NMSE (normalized mean square error); FB (fractional bias); Mod/Obs (modelled-observed ratio)

Scenario	**r** [a]	**NMSE**	**FB**	**Mod/Obs**
S1	**0.42**	3.11	0.76	2.24
S2	**0.25**	1.99	0.37	1.45
S3	**0.37**	2.08	0.44	1.57
S4	**0.19**	2.08	0.15	1.16
S5	**0.29**	8.26	1.24	4.27
S6	0.17	7.69	1.11	3.47
S7	**0.23**	7.73	1.13	3.61
S8	0.15	7.72	1.05	3.21

[a] Statistically significant r-values for 95% confidence level are highlighted in bold.

Table 5. Statistics obtained from the comparison between observed and simulated PM_{10}-bound Mn concentration values by site for best scenarios (dimensionless): r (correlation coefficient); NMSE (normalized mean square error); FB (fractional bias); Mod/Obs (modelled-observed ratio)

	S2				S3				S4			
Site	**CCV**	**CROS**	**CMFC**	**GUAR**	**CCV**	**CROS**	**CMFC**	**GUAR**	**CCV**	**CROS**	**CMFC**	**GUAR**
r	0.10	0.17	0.34	0.42	0.38	0.20	0.42	0.40	0.06	0.16	0.35	0.41
NMSE	1.19	1.86	0.93	9.92	1.35	1.70	0.84	9.69	1.14	2.09	0.89	9.67
FB	0.43	-0.01	0.24	1.29	0.73	-0.08	0.01	1.28	0.19	-0.24	-0.07	1.27
Mod/Obs	1.54	0.99	1.28	4.64	2.16	0.93	1.01	4.59	1.21	0.78	0.93	4.50

Table 6. Comparison between PM_{10}-bound observed and modelled Mn concentration values (ng/m^3) for selected scenarios.

		Arithmetic Mean				Standard Deviation				Median				Maximum			
		Obs	Mod			Obs	Mod			Obs	Mod			Obs	Mod		
	n		S2	S3	S4		S2	S3	S4		S2	S3	S4		S2	S3	S4
TOTAL	101	527	762	826	611	518	835	963	742	302	538	486	407	2,062	4,230	4,096	4,058
CCV	23	813	1,253	1,757	982	635	874	1,097	761	813	1,075	1,608	826	2,062	3,851	3,595	3,152
CROS	44	390	387	362	306	411	421	371	355	198	252	245	169	1,670	1,514	1,373	1,395
CMFC	23	682	818	648	596	571	648	573	491	577	623	461	417	1,859	2,748	2,466	1,801
GUAR	11	314	1,122	1,109	1,088	249	1,515	1,485	1,479	203	782	777	750	917	4,230	4,096	4,058

FIGURE CAPTIONS

Figure 1. Study area and wind rose for the studied period based on measurements from Guarnizo CIMA meteorological station.

Figure 2. Flow diagram of the ferromanganese alloy production and main air Mn emissions associated to each process.

Figure 3. Scatter plots of PM_{10}-bound Mn concentrations (ng/m^3): observed vs modelled values for all the monitoring sites.

Figure 4. Temporal variation of observed and modelled Mn concentrations by site.

Figure 5. Modelled daily average PM_{10} – bound Mn (ng/m^3) for S3 emission scenario: (a) 6/26/2015; (b) 9/13/2015; (c) 11/13/2015

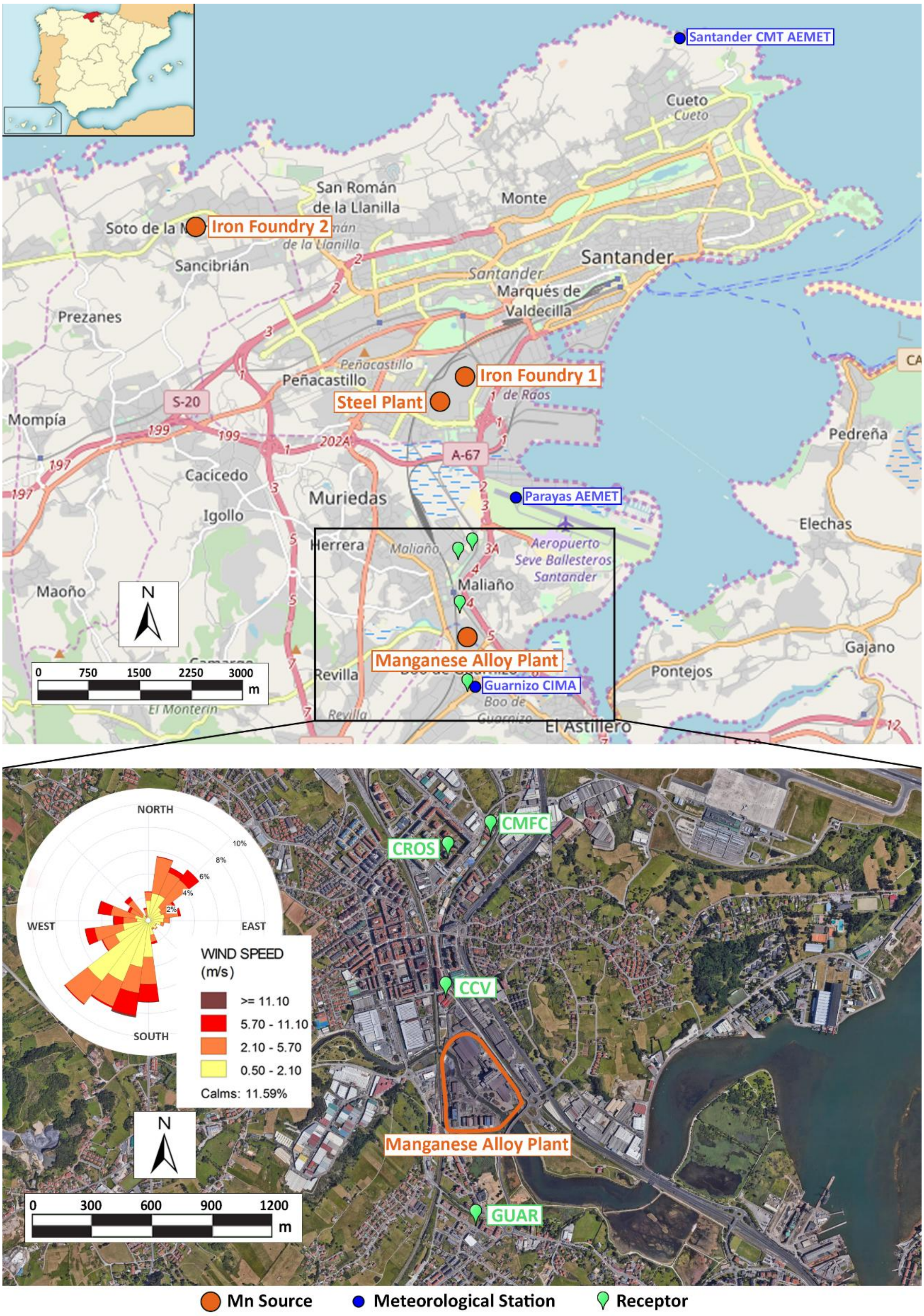

Figure 1. Study area and wind rose for the studied period based on measurements from Guarnizo CIMA meteorological station.

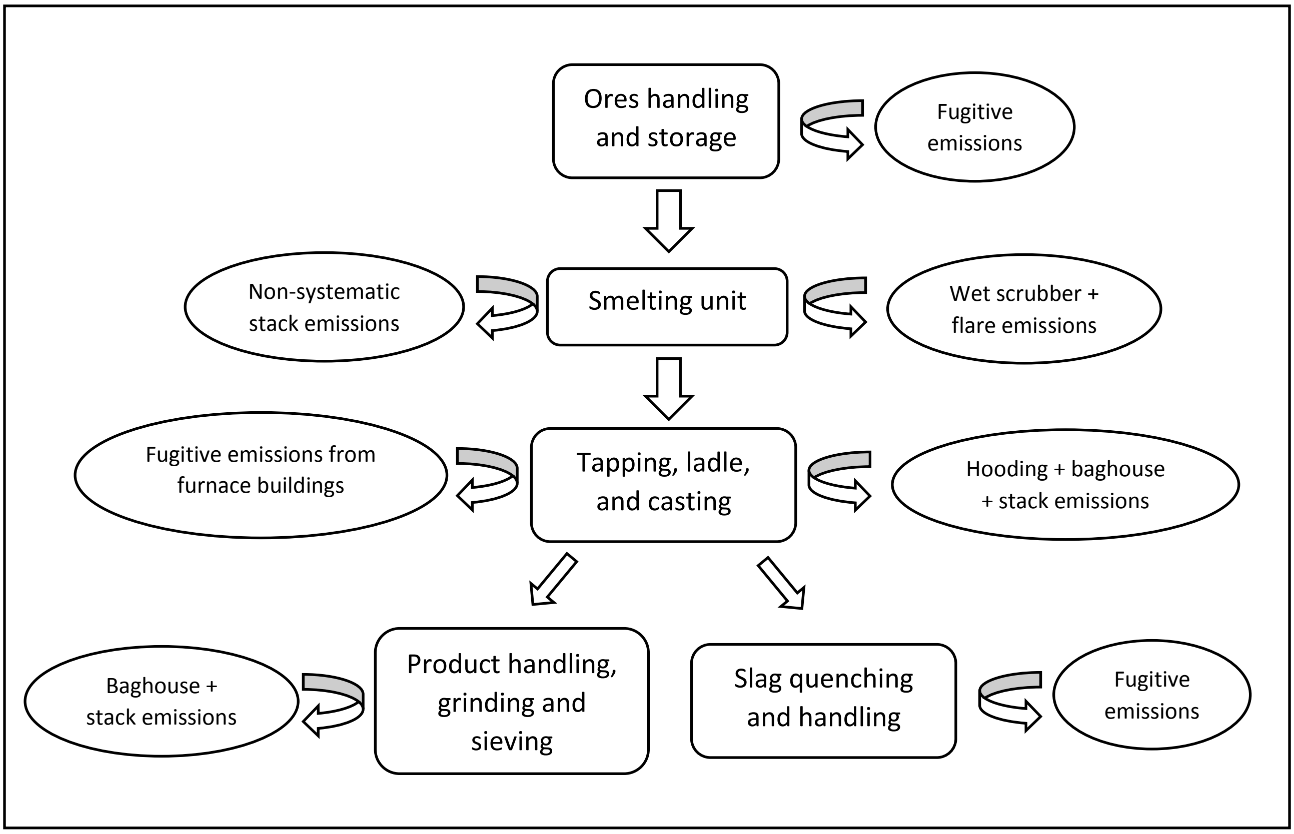

Figure 2. Flow diagram of the ferromanganese alloy production and main air Mn emissions associated to each process.

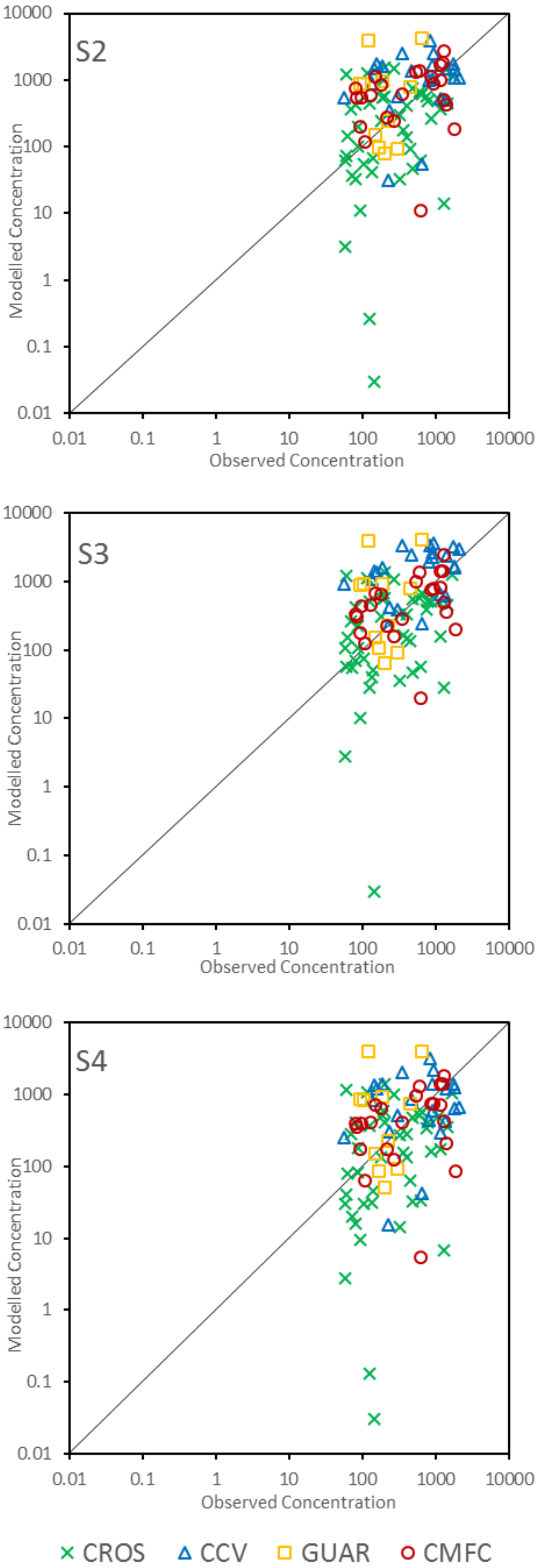

Figure 3. Scatter plots of PM_{10}-bound Mn concentrations (ng/m^3): observed vs modelled values for all the monitoring sites.

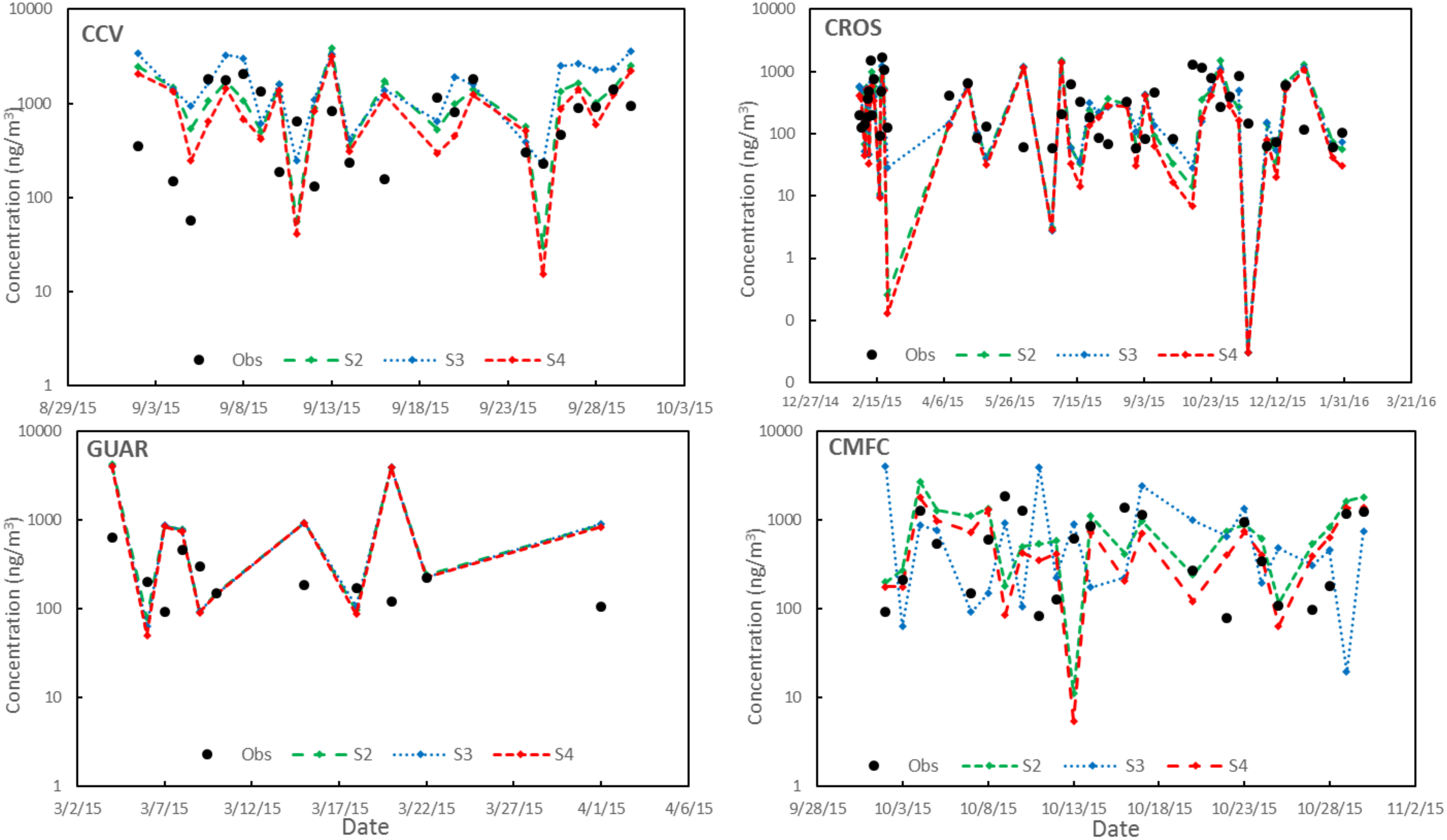

Figure 4. Temporal variation of observed and modelled Mn concentrations by site

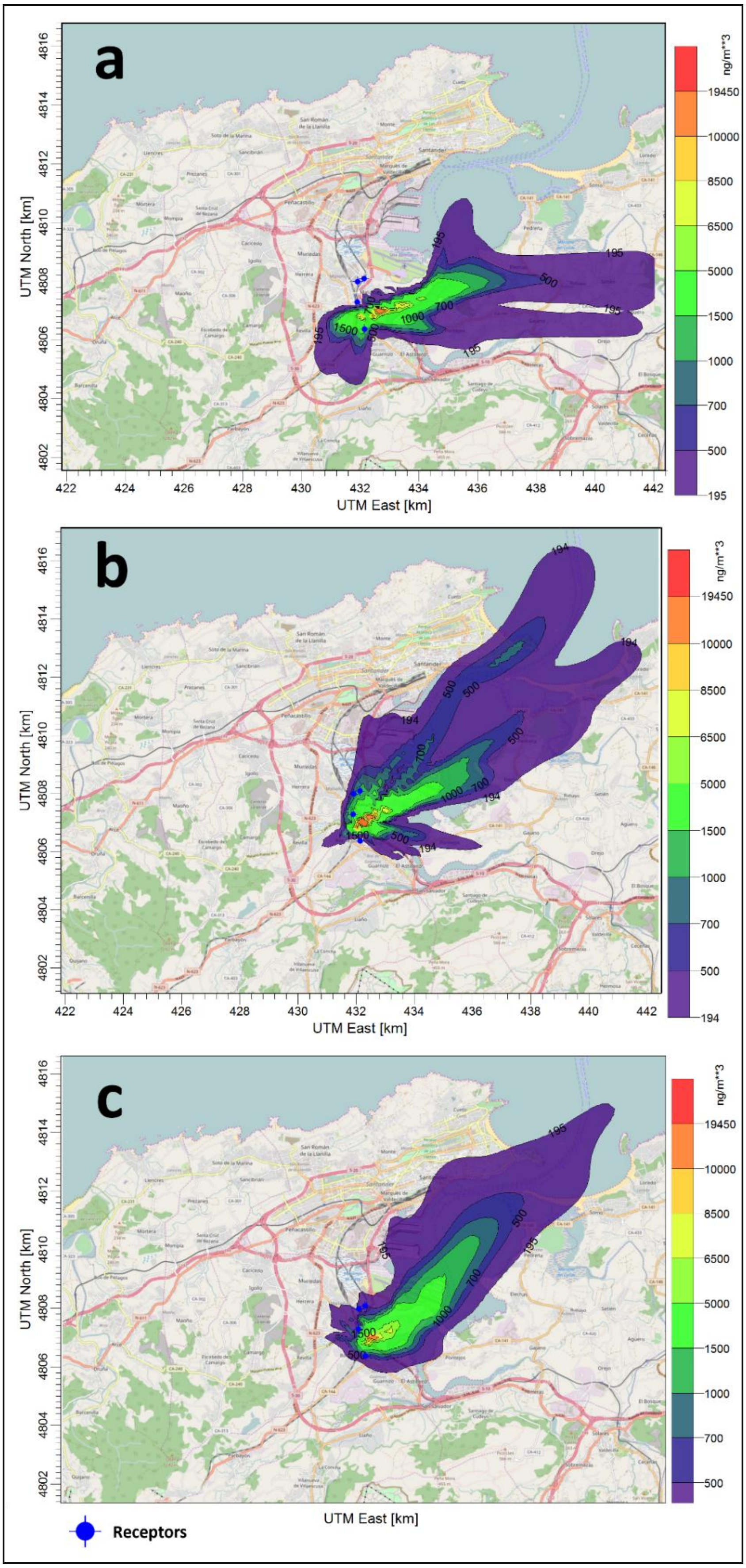
a
b
c
UTM North [km]
UTM East [km]
ng/m**3
19450
10000
8500
6500
5000
1500
1000
700
500
195
194
Receptors

Figure 5. Modelled daily average PM_{10} – bound Mn (ng/m^3) for S3 emission scenario: (a) 6/26/2015; (b) 9/13/2015; (c) 11/13/2015

SUPPLEMENTARY MATERIAL

Table S1. Emission factors used from US EPA (1984).

Operation	**FeMn**	**SiMn**	**Units**
Submerged-arc electric furnaces	0.038	0.001	kg Mn/MW·h
Ladle treatment	3.75	3	kg Mn/t
Casting	0.24	0.12	kg Mn/t
Crushing/grinding/sizing	0.08	0.065	kg Mn/t

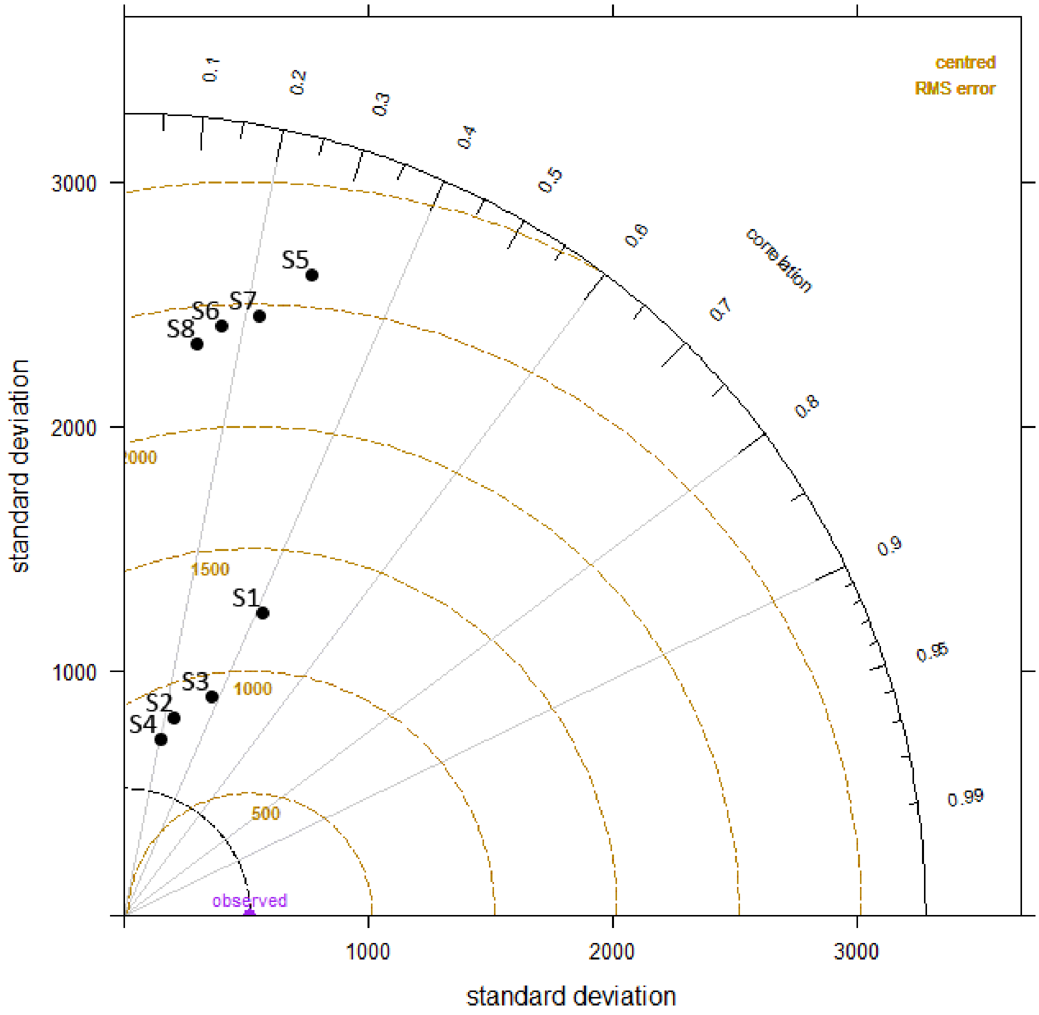

Figure S1: Model performance for all the scenarios considered.